IOP Publishing — Journal of Physics D: Applied Physics
J. Phys. D: Appl. Phys. **43** (2010) 325301 (8pp) doi:10.1088/0022-3727/43/32/325301

Ultrasonic friction power during thermosonic Au and Cu ball bonding

A Shah[1], M Mayer[1], I Qin[2], C Huynh[2], Y Zhou[1] and M Meyer[2]

[1] Microjoining Laboratory, University of Waterloo, ON, Canada
[2] Kulicke and Soffa Industries Inc., Fort Washington, PA, USA

E-mail: ashah011@engmail.uwaterloo.ca

Received 8 January 2010, in final form 29 June 2010
Published 29 July 2010
Online at stacks.iop.org/JPhysD/43/325301

Abstract
The ultrasonic friction power during thermosonic ball bonding with Au and Cu wires, both 25 μm in diameter, is derived with an improved method from experimental measurements during the bonding process. Experimental data include the current delivered to the ultrasonic transducer and the tangential force measured using piezoresistive microsensors integrated close to the Al bonding pad. The improvement results from a new, more accurate method to derive the mechanical compliance of the ultrasonic system. The method employs a bond process modification in which the ultrasonic current is ramped up sequentially in three steps. In the first two steps, the ultrasonic current is set to levels that are too low to cause sliding. The bonding takes place during the third step, when the current is ramped up to the optimum value required for making good quality bonds. The ultrasonic compliance values are derived from the first two steps and are $8.2 \pm 0.5\,\mu\mathrm{m\,N^{-1}}$ and $7.7 \pm 0.5\,\mu\mathrm{m\,N^{-1}}$ for the Au and Cu processes, respectively. These values are determined within an average error estimate of ±6%, substantially lower than the ±10% estimated with a previously reported method. The ultrasonic compliance in the case of Au is 6% higher due to the lower elastic modulus of Au compared with that of Cu. Typical maximum values of relative sliding amplitude of ultrasonic friction at the interface are 655 nm and 766 nm for the Au and Cu processes. These values are 81% of the free-air vibration amplitude of the bonding capillary tip for the respective ultrasonic current settings. Due to bond growth, which damps relative motion between the ball and the pad, the final relative amplitude at the bond interface is reduced to 4% of the equivalent free-air amplitude. Even though the maximum value of relative amplitude is 17% higher in the Cu process compared with the Au process, the average total interfacial sliding is 519 μm in the Cu process, which is 31% lower than that in the Au process (759 μm). The average maximum interfacial friction power is 10.3 mW and 16.9 mW for the Au and Cu ball bonding processes, respectively. The total sliding friction energy delivered to the bond is 48.5 μJ and 49.4 μJ for the Au and Cu ball bonding cases, respectively. These values result in average friction energy densities of 50.3 mJ mm^{-2} and 54.8 mJ mm^{-2} for Au and Cu ball bonding, respectively.

(Some figures in this article are in colour only in the electronic version)

Nomenclature

A_o	ultrasonic amplitude of the capillary tip measured in free air (in μm)
A_o^{max}	maximum value of A_o (in μm)
A_o^{nf}	ultrasonic amplitude when there is completely firm connection at the ball/pad interface (no friction) (in μm)
A_{rel}	relative sliding amplitude of ultrasonic friction (in μm)
A_{rel}^{max}	maximum value of A_{rel} (in μm)
A_T	total sliding distance (in μm)
BDI	nominal bonded ball diameter at interface (in μm)
c	ultrasonic compliance (in $\mu\mathrm{m\,N^{-1}}$)
ΔA_o^{nf}	error of A_o^{nf} (in μm)

 © 2010 IOP Publishing Ltd Printed in the UK & the USA

Δf_{calib}	error of $f_{calib} = 0.9\,\mathrm{mV\,V^{-1}\,N^{-1}}$
ΔM	error of M (in $\mathrm{mV\,V^{-1}}$)
E	total sliding friction energy delivered to the bond (in mJ)
f	ultrasonic frequency = 122.5 kHz
f_{calib}	calibration factor of the microsensor = $17.3\,\mathrm{mV\,V^{-1}\,N^{-1}}$
M	non-dimensional response of the microsensor (in $\mathrm{mV\,V^{-1}}$)
f_d	ultrasonic amplitude–transducer current calibration constant = $18.08\,\mathrm{nm\,mA^{-1}}$
F_t	ultrasonic tangential force acting at the bond interface and measured by the microsensor (mN)
F_t^{nf}	ultrasonic tangential force when there is completely firm connection at the ball/pad interface (no friction) (in mN)
I	transducer current (in mA)
I_{opt}	optimum value of I (in mA)
P	ultrasonic friction power (in mW)
P_{max}	maximum value of P (in mW)
S	nominal bonded ball interfacial area (in $\mu\mathrm{m}^2$)
S_{eff}	effective interfacial area (in $\mu\mathrm{m}^2$)
U_{rel}	relative sliding velocity (in $\mu\mathrm{m\,s^{-1}}$)

1. Introduction

Wire bonding is an essential process step in microelectronics packaging that provides for electrical interconnections between an integrated circuit (IC) and the external leads of a package. Among all the variants of wire bonding processes, the thermosonic Au wire ball bonding process is the most commonly employed method in the industry [1–3]. It is a solid state welding process in which a microwire loop is welded to a metallized surface on the IC using a capillary tool under a combined action of ultrasound, normal force and heat. The forces produce sliding friction at the contact zone between the wire and the pad (interface). This leads to some wear and then to the bond being established.

While the wire bonding process has been investigated in detail in the past, most studies are confined to a qualitative understanding of the bonding process only [4–12]. Detailed knowledge of the conditions at the interface is critical to develop a quantitative model of the bonding process. An approach to better understand the physics of the thermosonic bonding process [13] involves measuring the real time, *in situ* ultrasonic force acting at the bonding interface using piezoresistive sensors integrated close to the bond pad. The analysis of the harmonics of the ultrasonic force signal with Au [13–14], Cu [15–16] and Al [17] wires revealed that the relative stick–slip motion between the wire and pad at the interface is an important mechanism during these ultrasonic wire bonding variants.

The concept of stick–slip friction was further developed in [18] and a friction power model was formulated [19]. This model was extended by introducing a bond quality factor [20] and wire deformation during the process [21]. By measuring the ultrasonic tangential force, the current supplied to the ultrasonic transducer, and the free-air vibration amplitude of the tool, various characteristic coefficients, such as mechanical compliance (inverse stiffness) of the ultrasonic system and relative sliding amplitude at the interface were estimated [17]. These values were used to derive the ultrasonic friction power during ultrasonic Al wedge/wedge bonding on Al pads [17].

This paper reports on a new method to derive the transient ultrasonic friction power with improved accuracy and on results obtained during thermosonic Au and Cu ball bonding processes.

2. Theory of friction power

The formula for ultrasonic friction power P at the ball pad interface is [19]

$$P(t) = 4 \cdot A_{rel}(t) \cdot f \cdot F_t(t), \tag{1}$$

where A_{rel} is the zero-to-peak amplitude of relative motion between the ball and the pad, f is the ultrasonic frequency and F_t is the tangential force acting on the bond interface measured by the microsensor. Note that $A_{rel}(t)$ and $P(t)$ do not directly depend on the coefficient of friction in dry sliding. The sliding friction causes cleaning of the interfacial regions, which is followed by the formation of metallurgical connection (bonding) between the two mating surfaces (microwelds). The microwelds do not witness any sliding but shear yielding due to the ongoing ultrasound. The measured $F_t(t)$ includes the combined effect of coefficient of friction (static and dynamic) as well as the shear yielding due to metallurgical bonding, and $F_t(t)$ is the only signal used to determine $A_{rel}(t)$ and $P(t)$.

The value of A_{rel} is derived using a simplified model describing the interfacial friction during the wire bonding process [17]:

$$A_{rel}(t) = \begin{cases} A_o(t) - c \cdot F_t(t) & \text{if } cF_t < A_o, \\ 0 & \text{if } cF_t \geqslant A_o, \end{cases} \tag{2}$$

where A_o is the free-air vibration amplitude of the tool tip and c is the mechanical compliance of the ultrasonic system. The value of A_o is obtained from the transducer current I using

$$A_o(t) = f_d \cdot I(t), \tag{3}$$

where $f_d = 18.08\,\mathrm{nm\,mA^{-1}}$ is the calibration constant for capillary tool tip displacement depending on transducer current. The value of f_d is measured using laser measurements of the free-air vibration amplitude of the capillary tool tip for different values of I.

The ultrasonic compliance is a measure of the ultrasonic free vibration amplitude reduction at the ball/pad interface per unit tangential force acting at the interface. In the case of no sliding, it is given by

$$c = \frac{A_o^{nf}}{F_t^{nf}}, \tag{4}$$

where A_o^{nf} and F_t^{nf} are the ultrasonic amplitude and tangential force when there is a completely firm connection at the ball/pad interface. Figure 1 summarizes the procedure to

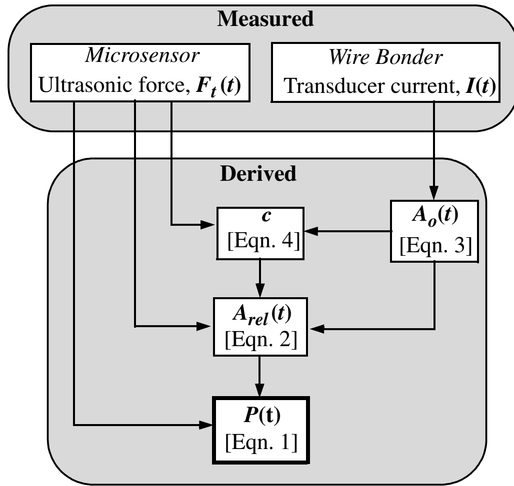

Figure 1. Schematic illustration outlining the procedure to derive P.

derive P. In contrast to the procedure described previously in [17], the procedure shown in figure 1 includes a new, direct and improved method to derive c. The experimental details and measurements required to derive P are described in the following sections.

3. Experimental

Thermosonic ball bonding is performed using 25 μm diameter Au and Cu wires on an automatic K&S IConn ball bonder (Kulicke and Soffa Industries Inc., Fort Washington, USA). This wire bonder uses a dual frequency transducer capable of producing ultrasonic vibrations at 50 and 122.5 kHz. In this study, $f = 122.5$ kHz is used. The nominal heater plate temperature is 150 °C, resulting in an actual temperature of ≈138 °C at the bond pad. A standard ceramic bottleneck capillary having a hole diameter of 30 μm and chamfer diameter of 35 μm is used. During the formation of free-air balls (FABs) with Cu wire, a homogeneous mixture of 95% nitrogen and 5% hydrogen is used as a shielding gas to prevent the oxidation of the hot FAB metal. The flow rate of the shielding gas is set to 0.62 l min^{-1}.

A test chip [15, 16] with integrated piezoresistive microsensors is used to measure the ultrasonic tangential force F_t acting at the bond interface. The design and operation of the microsensor and the various electrical components integrated in the test chip are explained in detail in [14–16]. The test chip is die bonded to a 16-pin SOIC package using a commercial silver filled epoxy, which then is cured at 150 °C for 90 min. The connection pads to the microsensor are connected to the package terminals by Au wire bonds. The package terminals are then soldered to a printed circuit board (PCB) as shown in figure 2. The PCB is placed on a custom-made heater plate and clamped by the vacuum system on the bonding machine.

3.1. Bonding process with modification

The ball bonding parameters are optimized on a chip with Al metallized bond pads using Au and Cu wires. A 35 μm diameter FAB is used for bonding using an impact deformation

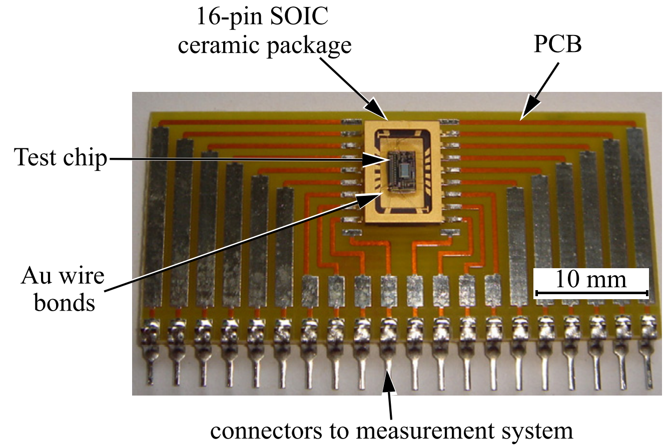

Figure 2. Microsensor test chip in package. Au wire bonds connecting to package terminals.

Table 1. Optimized ball bonding parameters and responses.

Parameter/response	Au	Cu
Impact force (a.u.)	10	16
Bond force, BF (gf)	14	16.25
Time (ms)	10	10
Ultrasonic current, I_{opt} (mA)	90	105
Ball diameter, BDI (μm)	35.0 ± 0.2	33.9 ± 0.7
Ball height, BH (μm)	8.6 ± 0.7	11.2 ± 0.7
Shear strength, SS (MPa)	99.8 ± 6.2	102.3 ± 8.1

(ID) process [22]. In an ID process, a two-stage normal force profile is used in which a high impact force precedes the bonding force. The impact force is used to deform the FAB to the desired bonded ball geometry. The ultrasound is used only for bonding and does not contribute to ball deformation. The optimized process parameters together with the obtained process responses for both wire types are shown in table 1. The nominal interfacial area is derived using $S = (\pi \cdot \mathrm{BDI}^2)/4$, where BDI is the bonded ball diameter at the interface (table 1). The estimated values of S for Au and Cu ball bonding are

$$S_{Au} = 960 \pm 13\ \mu\mathrm{m}^2, \tag{5}$$

$$S_{Cu} = 906 \pm 39\ \mu\mathrm{m}^2. \tag{6}$$

Thus, the average normal stress acting at the interface due to the bond force (table 1) is 143.1±1.9 MPa and 176.3±7.8 MPa for the Au and Cu processes, respectively.

To find the compliance values c using equation (4), the vibration amplitude and tangential force are evaluated for the case when there is no sliding at the interface. To this end, the bonding process is modified as shown by the illustration in figure 3 and the ultrasonic current profiles in table 2. The ultrasonic period is split into three segments. The duration and ultrasonic current for each segment is adjusted separately to obtain two low level ultrasonic steps before actual bonding, i.e. in segments 1 and 2, the value of ultrasonic current is set to relatively low values of 10% and 20% of the optimum ultrasonic parameter, I_{opt}, in order to prevent sliding friction at the ball/pad interface. Thus, bond formation takes place only during segment 3 when the ultrasonic current is ramped

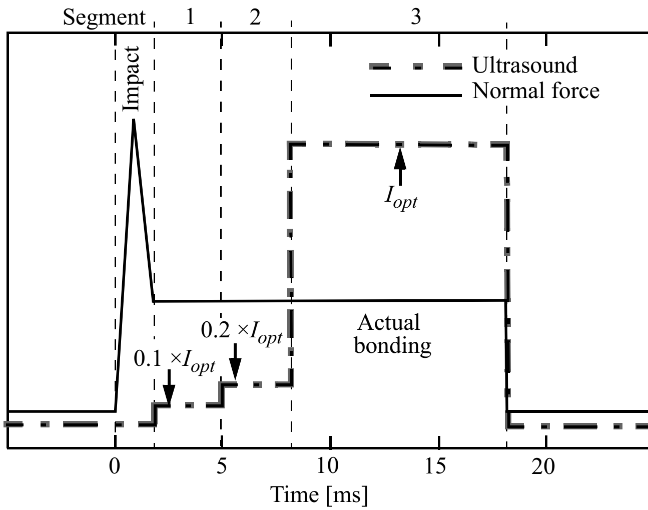

Figure 3. Schematic illustration of force and ultrasound profiles for the ball bonding tests.

Table 2. Ultrasonic current profile for ball bonding tests on the microsensor.

		Segment number			
			Bonding		
Wire type	Parameter	Impact	1	2	3
	Time (ms)	2	3	3	10
Au	Ultrasonic current (mA)	0	9	18	90
Cu		0	10.5	21	105

up to I_{opt}. All other bonding parameters are maintained at the optimized values shown in table 1.

The previous method [17] to derive c involved an estimation of the value of A_o^{nf} and F_t^{nf}. While the value of F_t^{nf} was taken at the break-off (onset of friction) in $F_t(t)$, the value of A_o^{nf} was estimated from $A_o(t)$ at the same time stamp as F_t^{nf}. Given the large rising slopes of both $F_t(t)$ and $A_o(t)$, and the fact that there is a small time delay between the two signals, the previous method results in a substantial error. Another drawback of the previous method is the ultrasonic enhanced deformation (UED) process [21] used in the study. In an UED process, the ultrasonic amplitude causes plastic deformation of the wire during the bonding process. This leads to a flattening of the wire, resulting in a reduction in the value of c during the bonding process. In contrast, the new method described here overcomes the drawbacks of the previous method by (i) more accurately deriving the values of A_o^{nf} and F_t^{nf} by the bond process modification using the two dedicated ultrasonic steps and (ii) using the ID process [22], which ensures that the changes in the value of c due to UED are minimized.

Ball bonding tests are performed with Au and Cu wires on the microsensor test pad and the real-time signals of F_t and I are measured simultaneously. The measurements are repeated six times for each wire type using the modified bonding process. Example of SEM micrographs of typical Au and Cu ball bonds on the test pad of the microsensor are shown in figures 4(*a*) and (*b*), respectively.

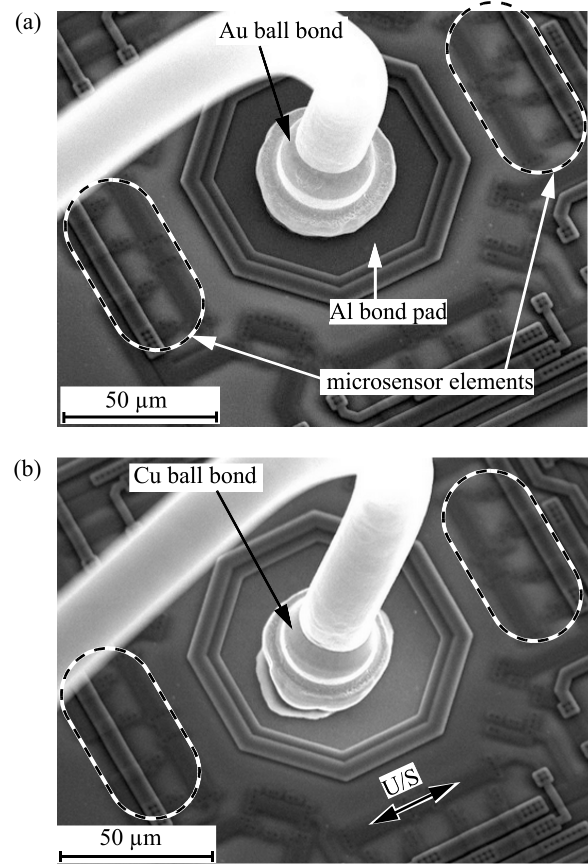

Figure 4. SEM micrographs of (*a*) Au and (*b*) Cu ball bonds on the microsensor test pad.

4. Results and discussion

4.1. Ultrasonic signals

The fundamental (first harmonic) and third harmonic amplitudes of F_t measured during typical Au and Cu ball bonding are shown in figures 5(*a*) and (*b*), respectively. The signal features are similar to those described previously for the Au [13] and Cu [15] ball bonding processes. The characteristic signal break-off in the first harmonic of F_t is observed in the Au signal, marking the onset of friction at the interface [13]. The onset of friction can also be determined from the time at which the third harmonic starts to rise.

Note that in this study, the zero-to-peak amplitude of F_t is approximated by its first harmonic. This approximation results in a small error as the higher harmonics will reduce the effective value of F_t. This is the case for the friction process signal modulation shape, i.e. cropped sine waveform [13–15] or asymmetric sine waveform [17]. However, this correction will only be significant for very strong friction processes. In this case, it might possibly cause several per cent deviation.

The zero-to-peak amplitudes of I are shown in figures 6(*a*) and (*b*) for Au and Cu ball bonding, respectively. A small time delay is observed between the I and the F_t signals, with F_t lagging behind I by $\approx 50\,\mu$s. Using equation (3), the corresponding values of A_o are derived and shown on the right-hand axis in figures 6(*a*) and (*b*). The current in the piezoelectric ceramics in the ultrasonic

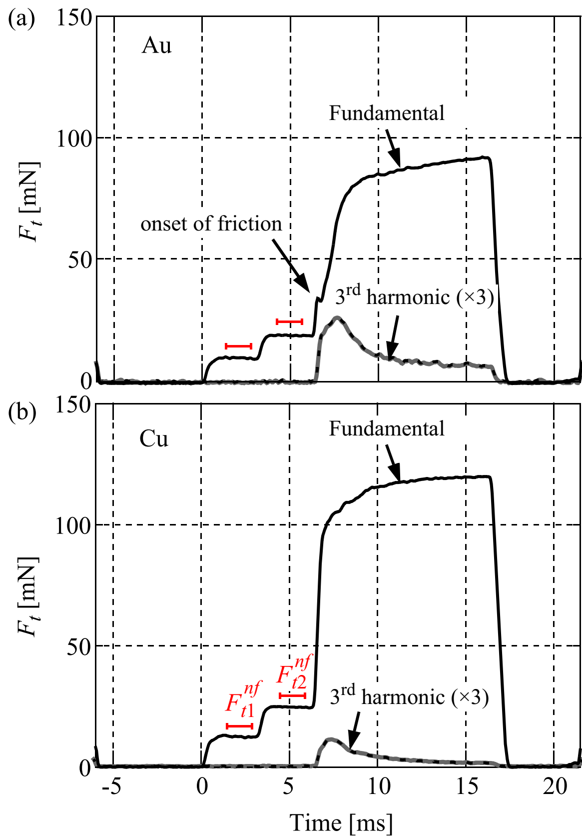

Figure 5. Typical fundamental and third harmonic amplitudes of $F_t(t)$ of (*a*) Au and (*b*) Cu ball bonding processes. The horizontal bars indicate the location at which average values of F_{tl}^{nf} are evaluated.

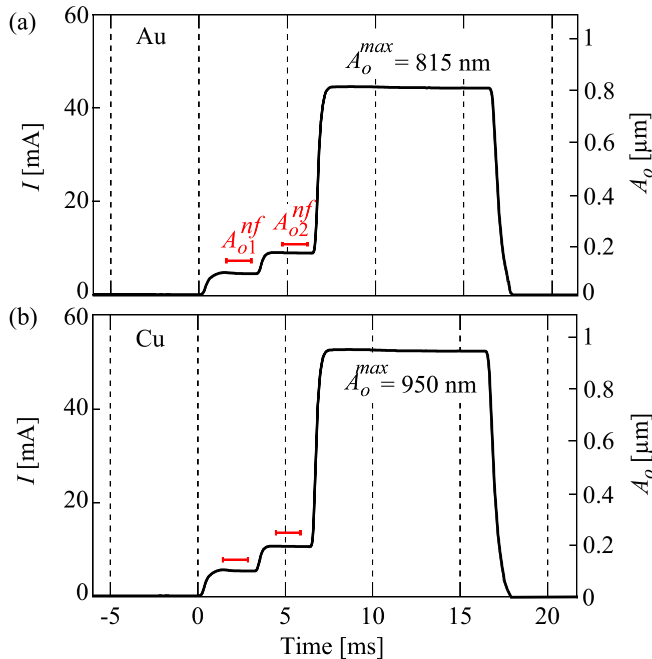

Figure 6. Transducer current I (t) and corresponding free capillary tool tip amplitude A_o (t) for parameter profiles used in (*a*) Au and (*b*) Cu ball bonding. The horizontal bars indicate the location at which average values of A_{oi}^{nf} are evaluated.

transducer during the bonding process is equal to that in free-air operation. This is provided by the constant current control used on this wire bonder, which automatically compensates for damping losses [17] during the bonding process.

4.2. Ultrasonic compliance

The values of F_t^{nf} and A_o^{nf} are evaluated from the steps in the plots of F_t and A_o (figures 5 and 6) at the periods indicated by horizontal bars in figures 5 and 6. By substituting these values in equation (4), the ultrasonic compliance for each segment is derived. The average values of c for the Au and Cu processes do not significantly depend on the step number. The overall averages ± standard deviations are 8.20 ± 0.18 and 7.66 ± 0.15 μm N^{-1}, respectively. Note that the error term is the sample standard deviation; it does not include the calibration error of the microsensor [16]. The overall error of c, Δc is

$$\Delta c = \left[\left(\frac{\Delta A_o^{nf} \cdot f_{calib}}{M} \right)^2 + \left(\frac{A_o^{nf} \cdot \Delta f_{calib}}{M} \right)^2 + \left(\frac{A_o^{nf} \cdot f_{calib} \cdot \Delta M}{M^2} \right)^2 \right]^{1/2}, \quad (7)$$

where ΔA_o^{nf} is the error of A_o^{nf}, M is the non-dimensional response of the microsensor (in mV V^{-1}), ΔM is the error of M (in mV V^{-1}) and $f_{calib} \pm \Delta f_{calib} = 17.3 \pm 0.9$ mV V^{-1} N^{-1} is the calibration factor ± error of the microsensor [16]. The overall error of c is $\Delta c = 0.51\,\mu$m N^{-1} for both Au and Cu processes. This value is 6% of the average when using the current method, compared with 10% determined for the previously reported method [17].

The values of c derived here are at least three times as large as those reported for the Al wedge bonding [17] and Au ball bonding [19] processes. Differences in the design of ultrasonic transducer, capillary tool, clamping and mechatronics control system on this wire bonder might be the reasons for the relatively large values of c.

It is observed that the compliance is 6–7% higher for the Au than for the Cu ball bonding process. This is due to the fact that Cu has an elastic modulus of 110–128 GPa which is 30–40% higher than that of Au [23]. It therefore offers an increased resistance to ultrasonic vibrations, resulting in lower compliance.

4.3. Relative sliding amplitude

The transient curves of A_{rel} derived using equation (2) for typical examples of the Au and Cu processes are shown in figures 7(*a*) and (*b*), respectively. The value of A_{rel} rapidly rises to a maximum value A_{rel}^{max} as soon as the ultrasonic dissipation starts. Then it starts to decrease. This decrease is indicative of bond growth, which reduces the relative motion at the interface. While the decrease is gradual during the Au process, it is more rapid during the Cu process. Moreover, a local maximum in A_{rel} is observed only for the Au process. The local maximum occurs approximately at the same time as the characteristic break-off observed in F_t (onset of friction) (figure 5(*a*)). One reason for this might be the mechanical

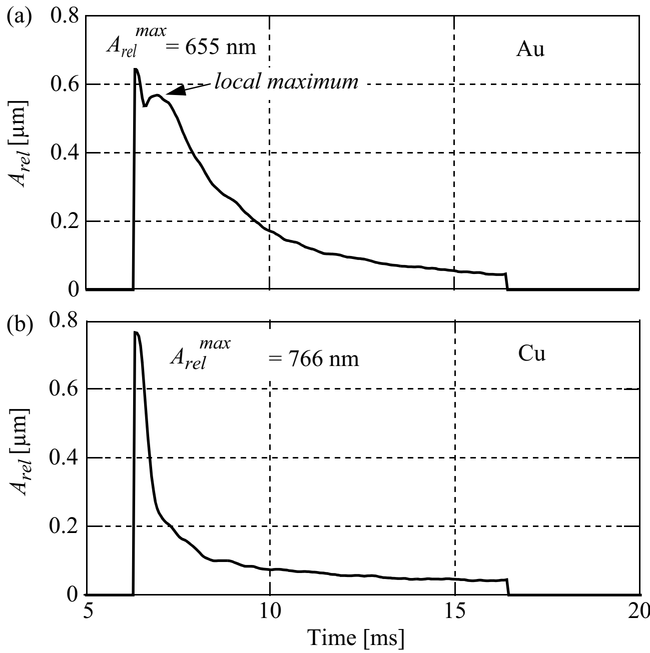

Figure 7. Relative sliding amplitude $A_{\mathrm{rel}}(t)$ for (*a*) Au and (*b*) Cu ball bonding processes.

interlocking between the Au ball and Al pad caused by the ID pressing the FAB onto the pad, preceding the ultrasonic period. The interlocking inhibits relative sliding at the interface for ≈0.5 ms as indicated by the local minimum (preceding the local maximum) in A_{rel}. However, it is not clear why this effect would be absent in the Cu ball bond process. Another reason might be attributed to a not yet understood tribological mechanism during Au ball bonding on Al, which results in a situation where a higher value of A_{rel} is temporarily induced at the interface for a lower value of F_{t}. This contradicts the mechanical interlocking mechanism described earlier. It is not completely clear which of these two reasons might be the cause for the local maximum in A_{rel}.

The average ± standard deviation of $A_{\mathrm{rel}}^{\mathrm{max}}$ are 654.4 ± 4.3 nm and 766.5 ± 1.4 nm for the Au and Cu processes, respectively. These values are 80.6% of the $A_{\mathrm{o}}^{\mathrm{max}}$, indicating that at least 19.4% of applied ultrasonic amplitude is lost due to friction at the beginning of the bonding process. Due to bond growth, which inhibits relative motion at the interface, the value of A_{rel} decreases to 35 nm at the end of the bonding process, indicating that the final clamped amplitude at the bond interface is only 4% of $A_{\mathrm{o}}^{\mathrm{max}}$.

The total sliding distance, A_{T}, is

$$A_{\mathrm{T}} = \int_0^t U_{\mathrm{rel}}(t)\mathrm{d}t, \tag{8}$$

where $U_{\mathrm{rel}}(t)$ is the relative sliding velocity averaged over one vibration cycle, given by

$$U_{\mathrm{rel}}(t) = 4 \cdot f \cdot A_{\mathrm{rel}}(t). \tag{9}$$

The average ± standard deviation of total sliding distance A_{T} derived using equation (8) is 758.6 ± 183.5 μm and 519.4 ± 36.1 μm for the Au and Cu ball bonding processes, respectively. Therefore, even though the values of $A_{\mathrm{o}}^{\mathrm{max}}$ and $A_{\mathrm{rel}}^{\mathrm{max}}$ for the Cu process are both ≈17% higher than the Au process, the total sliding A_{T} in the Cu process is found to be ≈31% lower than in the Au process. This finding supports the earlier conclusion of reduced sliding (friction) in Cu compared with Au obtained from the analysis of third harmonic of F_{t} of Au and Cu ball bonding [15].

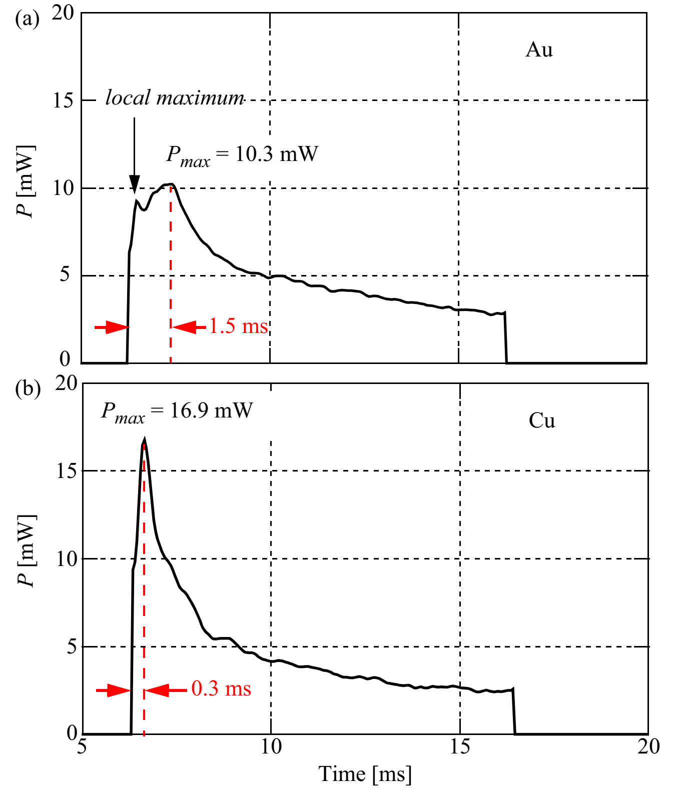

Figure 8. Ultrasonic friction power $P(t)$ for (*a*) Au and (*b*) Cu ball bonding processes.

4.4. Ultrasonic friction power

The ultrasonic friction power $P(t)$ evaluated using equation (1) for Au and Cu ball bonding are shown in figures 8(*a*) and (*b*), respectively. These curves are not exactly similar to those obtained during the Al wedge bonding process [17]. While the $P(t)$ curve for the Al wedge bonding process becomes zero within a few milliseconds after reaching the maximum value [17], the $P(t)$ curves for the Au and Cu ball bonding processes reach a non-zero steady-state value. The reason for $P(t)$ going to zero in the Al wedge bonding process was related to the end of friction (EOF) [24] at the wire/pad interface [25]. It is not completely clear why EOF might be absent in a ball bonding process, i.e. why $P(t)$ does not drop to zero before ultrasonic period ends. The maximum friction power (P_{max}) is a characteristic of the friction process at the ball/pad interface. The time stamp of P_{max} might indicate the high time of the cleaning process (removal of native oxides) at the ball/pad interface, which is a pre-requisite to high quality bond formation. The average maximum friction power P_{max} measured during the Cu process is 16.9 ± 0.3 mW, which is ≈64% higher than that measured during the Au process

(10.3 ± 0.1 mW). The time required to reach P_{max} is measured from the start of actual bonding (third segment in figure 3), and is 0.3 ms for the Cu process. This is ≈1.2 ms less than in the Au process. This is consistent with reports on faster bond growth in a Cu process compared with a Au process [15].

The decrease in $P(t)$ can be explained using the concept of real or effective interfacial area [26–31]. Since most engineering surfaces are rough at the microscopic scale, the effective interfacial area S_{eff} is only a fraction of the nominal interfacial area S. The effective interfacial area S_{eff} is defined by the contact of the asperity tips of the two mating surfaces (ball and the pad). Due to friction power, the surface asperities are deformed (elastic and plastic) and cleaned (due to wear). This is accompanied by the formation of microwelds at the cleaned asperity contacts. With the ongoing ultrasound (increasing time t), S_{eff} increases, i.e. spreading of the microwelds to other parts of S. The ongoing ultrasound also causes shear yielding of these microwelds. The microwelds broken in the previous ultrasound cycle might be re-welded in the next ultrasound cycle, and this process continues until the end of the ultrasonic period. The growing S_{eff} causes damping of A_{rel}, leading to a corresponding decrease in $P(t)$. Note that the values of $A_{rel}(t)$ and $P(t)$ are derived using the measured $F_t(t)$. The tangential force $F_t(t)$ includes the effect of each of these physical processes, i.e. deformation of asperities, cleaning of native oxides, formation of microwelds (bonding) and shear yielding of the microwelds due to the ongoing ultrasound.

With the measured nominal interfacial areas (equations (5) and (6)), the average maximum friction power densities for the Au and Cu ball bonding processes are $10.8 \pm 0.2\,\mathrm{W\,mm^{-2}}$ and $18.7 \pm 0.6\,\mathrm{W\,mm^{-2}}$, respectively. These values are in the same order of magnitude as those reported for typical ultrasonic Al welding processes in the macroscopic range [32].

The total sliding friction energy delivered to the bond E is

$$E = \int_0^t P(t)\mathrm{d}t. \qquad (10)$$

The average values of E for Au and Cu ball bonding are $48.5 \pm 8.0\,\mu\mathrm{J}$ and $49.4 \pm 4.0\,\mu\mathrm{J}$, respectively. These values result in average friction energy densities of $50.3 \pm 7.8\,\mathrm{mJ\,mm^{-2}}$ and $54.8 \pm 4.8\,\mathrm{mJ\,mm^{-2}}$ for Au and Cu ball bonding, respectively.

5. Conclusions

The ultrasonic friction power is derived with improved accuracy for typical thermosonic ball bonding processes. The method uses the measured ultrasonic force and transducer current as inputs. To derive the friction power, the ultrasonic compliance of the bonding system and the relative sliding amplitude at the interface are determined first.

With the improved accuracy, friction power differences of processes with different materials can be quantified with greater significance. Differences in bonding mechanisms can now be detected in more detail, e.g. the interfacial tribological processes. It is found that the friction cleaning process in Cu ball bonding is faster than in Au, resulting in faster bond formation in a Cu process compared with an Au process.

In the future, deriving ultrasonic friction power will help to understand possible interactions between surface physics and joining mechanisms of the ultrasonic wire bonding process. For example, a more comprehensive model would include sliding wear [33] to study interfacial fretting during ultrasonic wire bonding. The theory might be extended to predict the bonding process parameters and bond strength [21], possibly leading to new control methodologies [34] and higher process quality.

Acknowledgments

This work is supported by the Natural Sciences and Engineering Research Council of Canada (NSERC), the Ontario Centers of Excellence (OCE), the Government of Canada's NSERC Alexander Graham Bell Canada Graduate Scholarship and the University of Waterloo President's Graduate Scholarship.

References

[1] Greig W J 2007 *Integrated Circuit Packaging, Assembly and Interconnections* (New York: Springer Science + Business Media)

[2] Harman G 1997 *Wire Bonding in Microelectronics: Materials, Processes, Reliability, and Yield* 2nd edn (New York: McGraw-Hill)

[3] Zhou Y (ed) 2008 *Microjoining and Nanojoining* (Cambridge, England: Woodhead Publishing Ltd)

[4] Harman G and Leedy K O 1972 An Experimental model of the microelectronic ultrasonic bonding mechanisms *Proc. 10th Annual Reliability Physics Symp. (Las Vegas, NV)* pp 49–56

[5] Harman G and Albers J 1977 The ultrasonic welding mechanism as applied to aluminum and gold wire bonding in microelectronics *IEEE Trans. Hybrids Packag.* **13** 406–12

[6] Joshi K C 1971 The formation of ultrasonic bonds between metals *Weld. J.* **50** 840–8

[7] Krzanowski J E 1990 A transmission electron microscopy study of ultrasonic wire bonding *IEEE Trans. Compon. Hybrids Manuf. Technol.* **13** 176–81

[8] Harthoorn J L 1973 Joint formation in US welding compared with fretting phenomena for aluminium *Proc. Int. Conf. on Ultrasonics (Guildford, UK)* pp 43–51

[9] Chen G 1972 The role of micro-slip in ultrasonic bonding of microelectronic dimensions *Proc. Int. Hybrid Microelectronics Symp.*

[10] Zhou N, Li X and Noolu N J 2005 A footprint study of bond initiation in gold wire crescent bonding *IEEE Trans. on Compon. Packag. Technol.* **28** 810–16

[11] Lum I, Jung J P and Zhou Y 2005 Bonding mechanism in ultrasonic gold ball bonds on copper substrate *Metall. Mater. Trans.* A **36A** 1279–86

[12] Lum I, Mayer M and Zhou Y 2006 Footprint study of ultrasonic wedge bonding with aluminium wire on copper substrate *J. Electron. Mater.* **35** 433–42

[13] Mayer M, Schwizer J, Paul O, Bolliger D and Baltes H 1999 *In situ* ultrasonic stress measurements during ball bonding using integrated piezoresistive microsensors *Advances in Electronic Packaging (Proc. InterPACK99 Conf.) (Dusseldorf)* vol 26-1 (ASME) pp 973–8

[14] Schwizer J, Mayer M and Brand O 2005 *Force Sensors for Microelectronic Packaging Applications* (Berlin: Springer)

[15] Shah A, Mayer M, Zhou Y, Hong S J and Moon J T 2008 *In situ* ultrasonic force signals during low-temperature thermosonic copper wire bonding *Microelectron. Eng.* **85** 1851–7

[16] Shah A, Mayer M, Zhou Y, Hong S J and Moon J T 2009 Low-stress thermosonic copper ball bonding *IEEE Trans. Electron. Packag. Manuf.* **32** 3

[17] Shah A, Gaul H, Schneider-Ramelow M, Reichl H, Mayer M and Zhou Y 2009 Ultrasonic friction power during Al wire wedge–wedge bonding *J. Appl. Phys.* **106** 013503-1/8

[18] Schwizer J, Mayer M, Bolliger D, Paul O and Baltes H 1999 Thermosonic ball bonding: friction model based on integrated microsensor measurements *Proc. IEEE/CPMT Int. Electronics Manufacturing Technology Symp. (Austin, TX)* pp 108–14

[19] Mayer M and Schwizer J 2002 Ultrasonic bonding: understanding how process parameters determine the strength of Au–Al bonds *Proc. IMAPS Int. Symp. on Microelectronics (Denver, CO)*

[20] Mayer M and Schwizer J 2003 Thermosonic ball bonding model based on ultrasonic friction power *Proc. IEEE Electronic Packaging Technology Conf. (Singapore)* pp 738–43

[21] Gaul H, Schneider-Ramelow M, Lang K-D and Reichl H 2006 Predicting the shear strength of a wire bond using laser vibration measurements *Proc. 1st Electronics Systemintegration Technology Conf. (Dresden)* vol 2, pp 719–25

[22] McKenna R G and Mahle R L 1989 High impact bonding to improve reliability of VLSI die in plastic packages *Proc. IEEE Electronic Components Conf.* pp 424–7

[23] 1990 *ASM Handbook vol 2 Properties and Selection: Nonferrous Alloys and Special Purpose Materials* 10th edn (ASM International)

[24] Gaul H, Schneider-Ramelow M and Reichl H 2009 Analysis of the friction processes in ultrasonic wedge/wedge bonding *Microsyst. Technol.* **15** 771–5

[25] Shah A 2010 Mechanical and tribological aspects of microelectronic wire bonding *PhD Thesis* University of Waterloo, Waterloo, Ontario, Canada, pp 77–9. Available online at: http://hdl.handle.net/10012/5109

[26] Jeng Y R and Horng J H 2001 A microcontact approach for ultrasonic wire bonding in microelectronics *Trans. ASME, J. Tribol.* **123** 725–31

[27] Jeng Y R and Chen C Y 2005 On the microcontact mechanism of thermosonic wire bonding in microelectronics: saturation of interfacial phenomena *STLE Tribol. Trans.* **48** 127–32

[28] Ding Y, Kim J K and Tong P 2006 Effects of bonding force on contact pressure and frictional energy in wire bonding *Microelectron. Reliab.* **46** 1101–12

[29] Jeng Y R, Aoh J N and Wang C M 2001 Thermosonic wire bonding of gold wire onto copper pad using the saturated interfacial phenomena *J. Phys. D: Appl. Phys.* **34** 3515–21

[30] Jeng Y R and Lin J N 2003 Study of interfacial phenomena affecting thermosonic wire bonding in microelectronics *Trans. ASME, J. Tribol.* **125** 578–81

[31] Gaul H, Shah A, Mayer M, Zhou Y, Schneider-Ramelow M and Reichl H 2001 The ultrasonic wedge/wedge bonding process investigated using *in situ* real-time amplitudes from laser vibrometer and integrated force sensor *Microelectron. Eng.* **87** 537–42

[32] Cheng X and Li A 2007 Investigation of heat generation in ultrasonic metal welding using microsensor arrays *J. Micromech. Microeng.* **17** 273–82

[33] Archard J F 1953 Contact and rubbing of flat surfaces *J. Appl. Phys.* **24** 981–8

[34] Geissler U, Reichl H, Gaul H, Lang K-D and Schneider-Ramelow 2008 Method and device for controlling the generation of ultrasonic wire bonds *European Patent Application* WO2008028906 (A1)